Supporting Information

WS_2 Nanosheets at Noncytotoxic Concentrations Enhance the Cytotoxicity of Organic Pollutants by Disturbing the Plasma Membrane and Efflux Pumps

Peng Yuan, Qixing Zhou*, Xiangang Hu

Key Laboratory of Pollution Processes and Environmental Criteria (Ministry of Education)/Tianjin Key Laboratory of Environmental Remediation and Pollution Control, College of Environmental Science and Engineering, Nankai University, Tianjin 300350, China.

Corresponding author: Qixing Zhou

Email: qxzhou523@163.com

Phone: 0086–022–23507800; fax: 0086–022–23507800.

Number of pages: 12

Number of figures: 9

Number of tables: 4

Quantification of TCS and TDCIPP in Cells

RAW264.7 and A549 cells were seeded in 24-well plates, cultured overnight and then exposed to TCS or TDCIPP with or without different concentrations of WS_2 nanosheets for 24 h. After washing with phosphate-buffered saline (PBS) three times to remove the organic pollutants that did not enter the cells or adhered to the cell surface, 1 mL of methanol was added, and ultrasound extraction was performed for 30 min to isolate the organic pollutants[1]. Then, the samples were filtered through a 0.22 μm filter membrane. TCS concentrations were determined using high-performance liquid chromatography (HPLC) according to a previous study[2]. The HPLC system comprised a binary HPLC pump (Waters 1525, USA), a Waters XTerra RP18 column (5 μm, 4.6 × 250 mm), an autosampler (Waters 717 Plus, USA), and a dual λ absorbance detector (Waters 2487, USA). The mobile phase consisted of methanol and water with a ratio of 90:10 (v/v) at a flow rate of 1 mL/min. The wavelength was set at 280 nm. TDCIPP concentrations were measured using ultra-performance liquid chromatography-tandem mass spectrometry (UPLC-MS) (OA_SPE Waters Xevo TQ-S, Waters, USA) according to a previous study[3]. Chromatographic separation was performed on a UPLC BEH C18 column (1.6 μm, 2.1 × 50 mm, Waters, USA), and water containing 2 mM ammonium acetate (A) and methanol (B) were used as mobile phases. Mass spectrometry was performed with electrospray ionization (ESI (+)) in the multiple reaction monitoring mode. TDCIPP was quantified using transitions of 430.9 > 99. Intracellular organic pollutant contents were normalized by the cell total protein.

Electron Microscope Observation

At the end of the exposure period, 1×10^6 RAW264.7 or A549 cells in each group were observed using scanning electron microscopy (SEM) and TEM. The cells were

first fixed in 2.5% glutaraldehyde overnight and then postfixed in 1% osmium tetroxide for 2 h. After dehydration with increasing ethanol concentrations, the samples were dried in a critical-point dryer. In preparation for SEM, the samples were sprayed with gold and visualized using a microscope (Hitachi SU8010, Japan). For TEM, the samples were embedded in an epoxy resin. Ultrathin sections of cells were obtained using an ultramicrotome and stained with uranyl acetate and lead citrate. Finally, the ultrathin sections were evaluated using high-resolution TEM (Hitachi HT7700, Japan).

Molecular Docking and Molecular Dynamics Simulations

The docking of TCS into the active sites of P-gp was determined by Libdocker software (Discovery Studio version 2.5, Accelrys, USA). As the human and mouse P-gp proteins show 87% overall sequence identity and nearly 100% identity of the binding cavity except for mSer725/hAla729, the mouse P-gp crystal structure (Protein Data Bank [PDB] code 3G60) was chosen as a representative receptor for molecular docking[4]. Water molecules were removed, and hydrogen atoms were added to P-gp. No specific reference active pocket was set, and a 15 Å docking radius was used to look for the site with the highest Libdock score. Molecular dynamics simulations were based on a general AMBER force field[5] with the RESP charges[6] and carried out using the Gromacs-4.6.7 software package[7]. The molecular structures are summarized in Table S1. The system was a relaxed liquid configuration at 298 K and 1 bar. A 2 ns canonical ensemble (NVT) relaxation run and a 2 ns constant-pressure, constant-temperature (NPT) relaxation run were performed before production simulation. The time step was 2 fs, and the total run time was 50 ns for the equilibrium molecular dynamics simulation. The relaxed system was used as a starting configuration. Prior to system relaxation in the molecular dynamics simulation, energy minimization was

carried out with a composite protocol of steepest descent using termination gradients of 100. The Nosé-Hoover thermostat[8] was used to maintain the equilibrium temperature at 298 K, and periodic boundary conditions were imposed on all three dimensions. The Particle Mesh-Ewald method[9] was used to compute long-range electrostatics within a relative tolerance of 1×10^{-6}. A cut-off distance of 1 nm was applied to real-space Ewald interactions. The same value was used for van der Waals interactions. The LINCS algorithm was applied to constrain the bond lengths of hydrogen atoms. A leap-frog algorithm was used with a time step of 2 fs. The secondary structure was calculated using the Define Secondary Structure of Proteins (DSSP) tool[10].

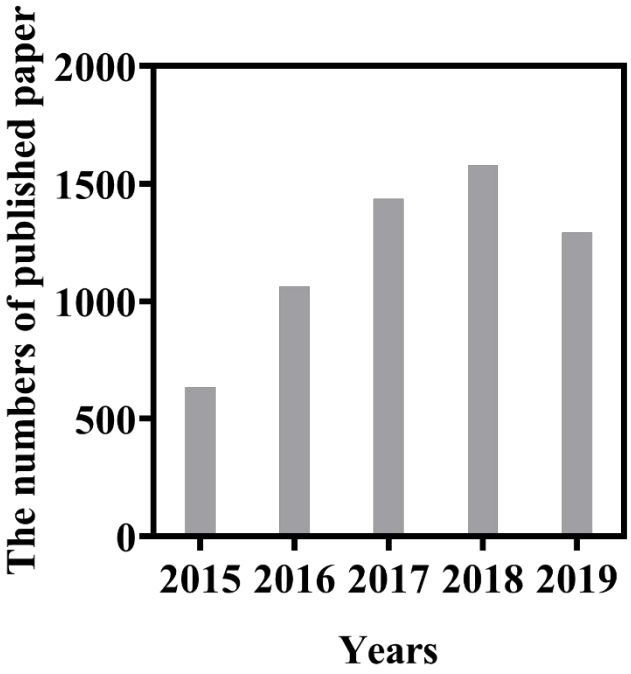

Figure S1. The numbers of published papers related to transition metal dichalcogenides in the past five years on Web of Science. The search date was 21 November 2019; the search topic was "transition metal dichalcogenides"; the years published were set from 2015 to 2019.

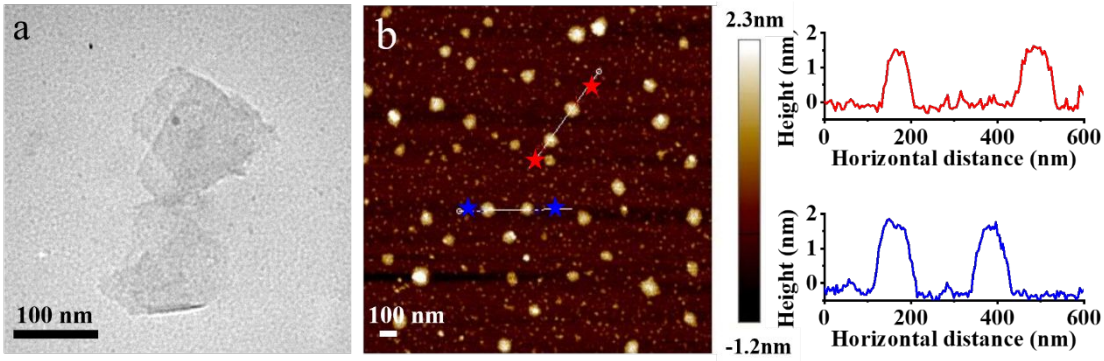

Figure S2. TEM images (a) and AFM images (b) of WS_2 nanosheets.

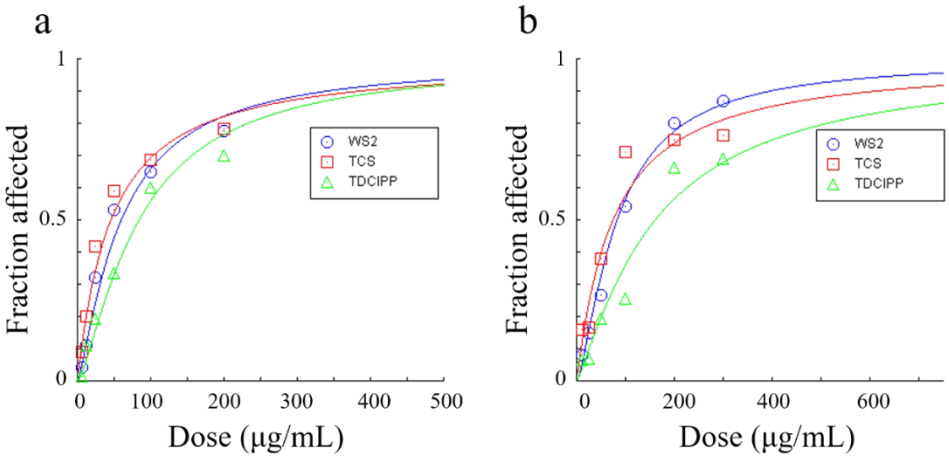

Figure S3. Dose-effect curves for WS_2 nanosheets, TCS and TDCIPP in RAW264.7 (a) and A549 (b) cells.

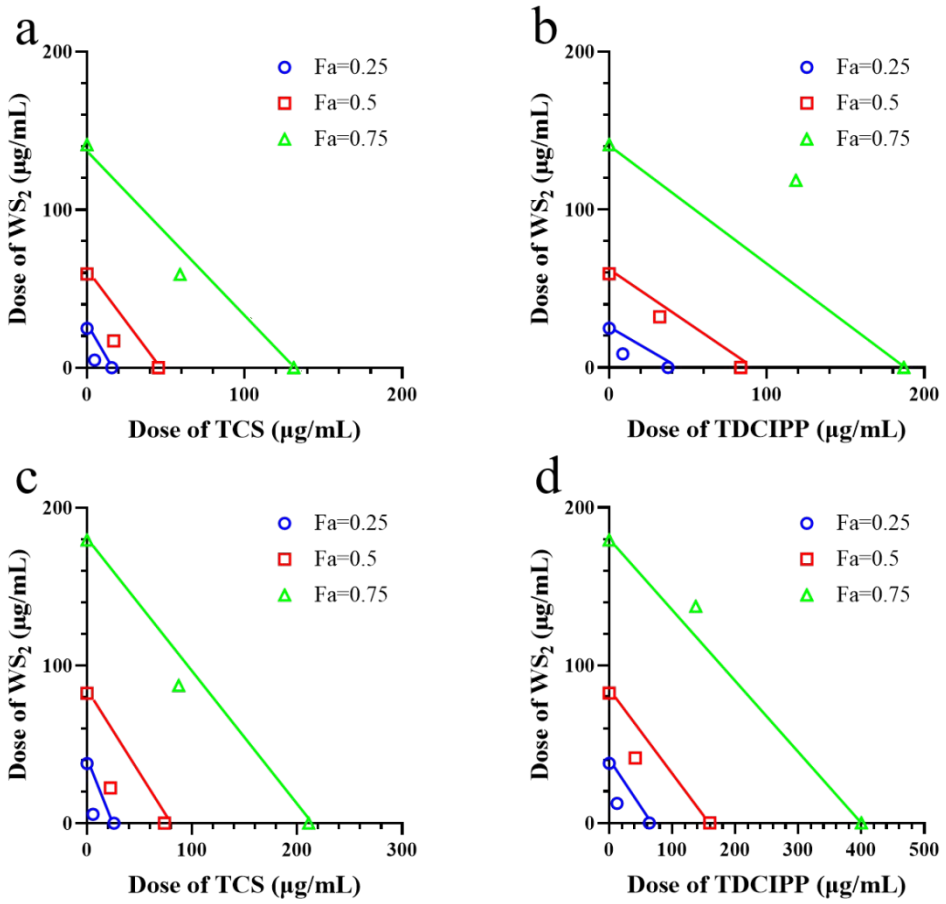

Figure S4. Isobologram of the combination cytotoxicity of WS_2 nanosheets and TCS (a, c) or TDCIPP (b, d) on RAW264.7 (a, b) and A549 (c, d) at the 25% (circle), 50% (square) or 75% (triangle) cytotoxicity level. Points located below, on and above the line indicate synergy, additivity and antagonism, respectively.

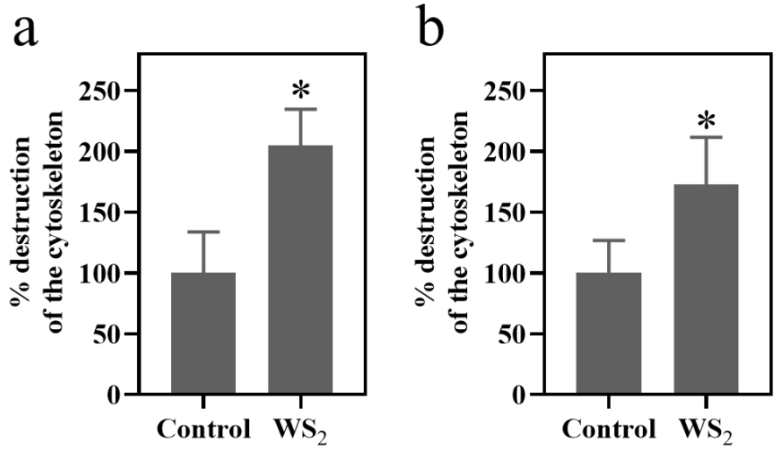

Figure S5. Quantitative analysis of cytoskeleton destruction in RAW264.7 (a) and A549 (b) cells. (n>100).

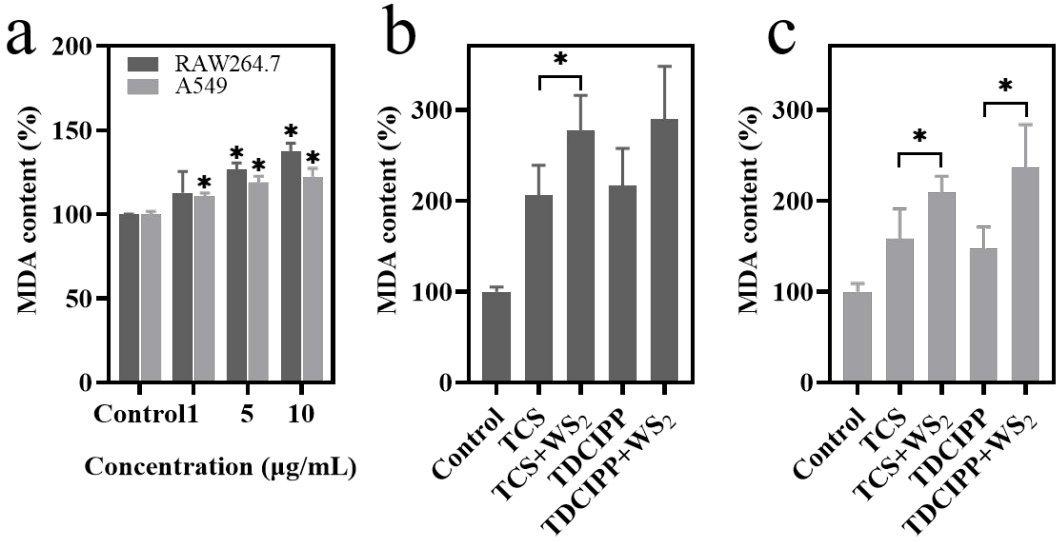

Figure S6. Lipid peroxidation of RAW264.7 and A549 cells. (a) The MDA content of RAW264.7 and A549 cells upon WS_2 nanosheet treatment for 24 h. The MDA content of RAW264.7 (b) and A549 cells (c) upon WS_2 nanosheet (10 μg/mL) and TCS (25 μg/mL) or TDCIPP (50 μg/mL) treatment for 24 h. "*" represents statistical significance at $p < 0.05$.

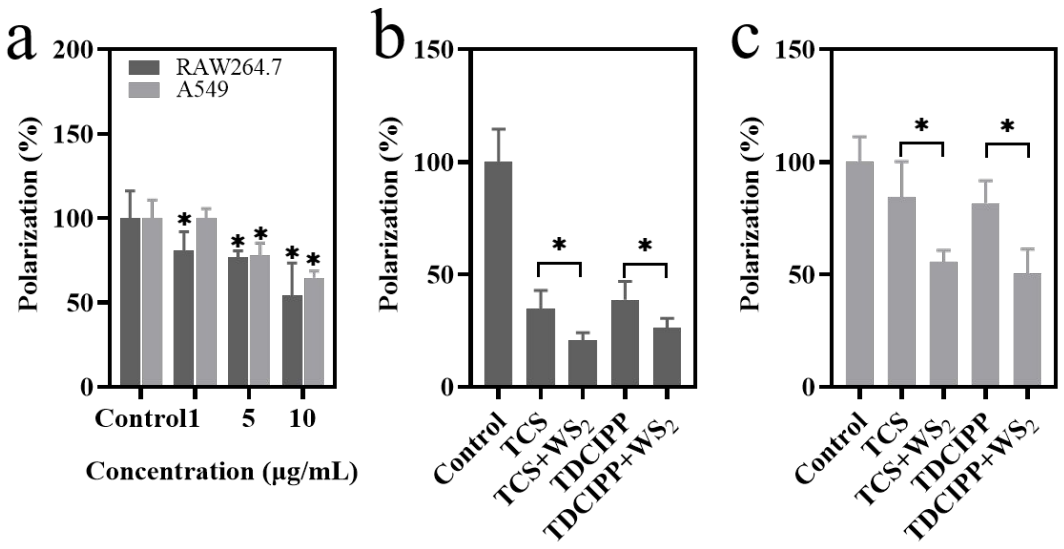

Figure S7. Membrane fluidity of RAW264.7 and A549 cells. (a) The polarization values of RAW264.7 and A549 cells after WS_2 nanosheet treatment for 24 h. The polarization values of RAW264.7 (b) and A549 cells (c) upon WS_2 nanosheet (10 μg/mL) and TCS (25 μg/mL) or TDCIPP (50 μg/mL) treatment for 24 h. "∗" represents statistical significance at $p < 0.05$.

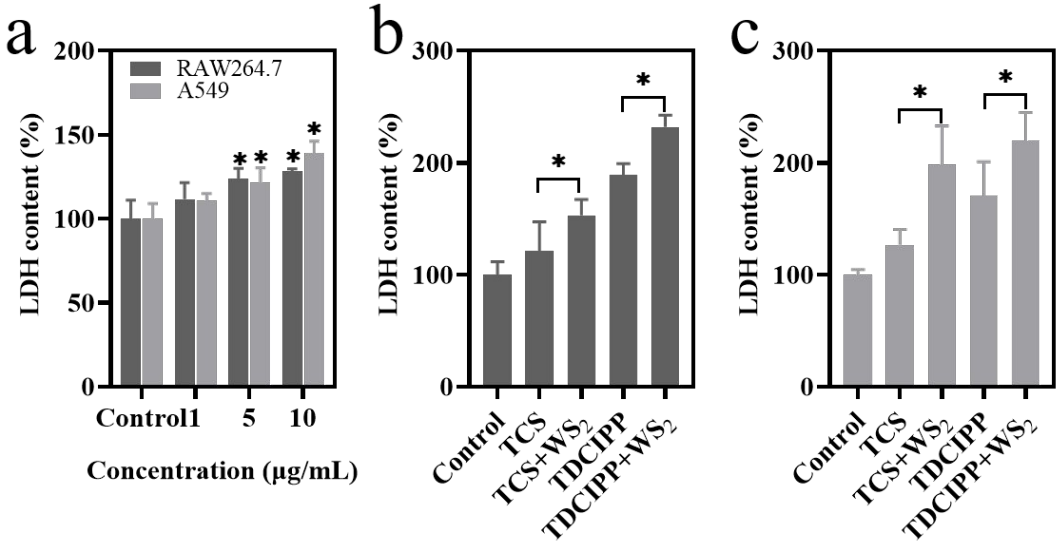

Figure S8. Membrane integrity of RAW264.7 and A549 cells. (a) The LDH content of RAW264.7 and A549 cells after WS_2 nanosheet treatment for 24 h. The LDH content of RAW264.7 (b) and A549 cells (c) after WS_2 nanosheet (10 μg/mL) and TCS (25 μg/mL) or TDCIPP (50 μg/mL) treatment for 24 h. "∗" represents statistical significance at $p < 0.05$.

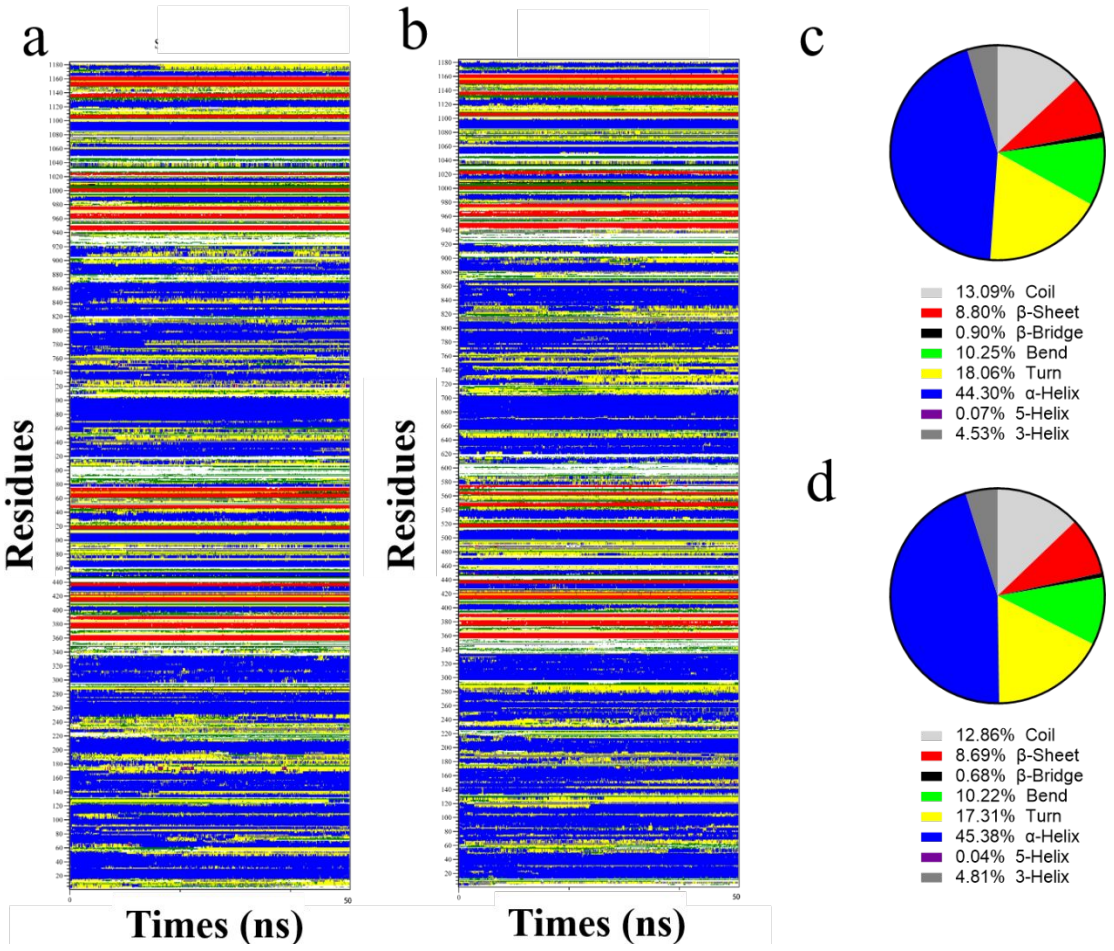

Figure S9. Time evolution of the secondary structure elements and ratio of all residues of P-gp without (a, c) and with (b, d) WS_2 nanosheets.

Table S1. Specifications of molecular dynamics simulation systems

	P-gp	WS_2 nanosheet	Water	NaCl (mmol/L)
System 1	1	-	112308	154
System 2	1	1	112265	154

Table S2. Hydrodynamic size and zeta-potential of WS_2 nanosheets in different media

	Medium	Value	pH
Hydrodynamic size (nm)	Deionized water	320.17 ± 16.57	
	PBS	1706.00 ± 128.00	
	DMEM (10% FBS)	303.40 ± 15.01	
Zeta-potential (mV)	Deionized water	-53.93 ± 5.37	7.05
	PBS	-15.13 ± 0.40	7.22
	DMEM (10% FBS)	-8.67 ± 0.70	8.09

Table S3. Dose-effect relationship parameters

Contaminants	Cell line	Dose-effect parameters		
		D_m (μg/mL)	m	r
WS_2 nanosheets	RAW264.7	59.29	1.27 ± 0.11	0.986
TCS		45.35	1.03 ± 0.09	0.985
TDCIPP		83.51	1.36 ± 0.15	0.975
WS_2 nanosheets + TCS		33.99	0.88 ± 0.07	0.987
WS_2 nanosheets + TDCIPP		64.25	0.84 ± 0.13	0.956
WS_2 nanosheets	A549	82.40	1.41 ± 0.08	0.994
TCS		73.81	1.05 ± 0.15	0.960
TDCIPP		159.67	1.20 ± 0.16	0.968
WS_2 nanosheets + TCS		44.79	0.81 ± 0.07	0.984
WS_2 nanosheets + TDCIPP		82.68	0.91 ± 0.06	0.991

D_m, m and r are the median-effect dose, the slope and the coefficient of linear correlation of the experimental data with regard to the mass-action law.

Table S4. Combination index and dose reduction index

Contaminants	Cells	25% Cytotoxicity		50% Cytotoxicity		75% Cytotoxicity	
		CI	DRI	CI	DRI	CI	DRI
WS_2 nanosheets	RAW264.7	0.51	5.10	0.66	3.49	0.87	2.39
TCS			3.21		2.67		2.22
WS_2 nanosheets	RAW264.7	0.58	2.86	0.93	1.85	1.47	1.19
TDCIPP			4.28		2.60		1.58
WS_2 nanosheets	A549	0.37	6.58	0.58	3.68	0.90	2.06
TCS			4.49		3.30		2.42
WS_2 nanosheets	A549	0.52	3.04	0.76	1.99	1.11	1.31
TDCIPP			5.12		3.86		2.91

CI, combination index. CI < 1, 0.9 = 1, and CI > 1 indicate synergism, additive effect, and antagonism, respectively. DRI, Dose reduction index.

REFERENCES

1. Albero, B.; Tadeo, J. L.; Pérez, R. A., Ultrasound-assisted extraction of organic contaminants. *Trac-Trends Anal. Chem.* **2019,** *118*, 739-750.

2. Proia, L.; Morin, S.; Peipoch, M.; Romaní, A. M.; Sabater, S., Resistance and recovery of river biofilms receiving short pulses of Triclosan and Diuron. *Sci. Total Environ.* **2011,** *409* (17), 3129-3137.

3. Li, H.; Su, G.; Zou, M.; Yu, L.; Letcher, R. J.; Yu, H.; Giesy, J. P.; Zhou, B.; Liu, C., Effects of tris(1,3-dichloro-2-propyl) phosphate on growth, reproduction, and gene transcription of *Daphnia magna* at environmentally relevant concentrations. *Environ Sci Technol* **2015,** *49* (21), 12975-12983.

4. Dolghih, E.; Bryant, C.; Renslo, A. R.; Jacobson, M. P., Predicting binding to P-glycoprotein by flexible receptor docking. *PLoS Comput. Biol.* **2011,** *7* (6), e1002083.

5. Wang, J.; Wolf, R. M.; Caldwell, J. W.; Kollman, P. A.; Case, D. A., Development and testing of a general amber force field. *J. Comput. Chem.* **2004,** *25* (9), 1157-1174.

6. Bayly, C. I.; Cieplak, P.; Cornell, W.; Kollman, P. A., A well-behaved electrostatic potential based method using charge restraints for deriving atomic charges: the RESP model. *J. Phys. Chem.* **1993,** *97* (40), 10269-10280.

7. Hess, B.; Kutzner, C.; Van Der Spoel, D.; Lindahl, E., GROMACS 4: algorithms for highly efficient, load-balanced, and scalable molecular simulation. *J. Chem. Theory Comput.* **2008,** *4* (3), 435-447.

8. Berendsen, H. J.; Postma, J. v.; van Gunsteren, W. F.; DiNola, A.; Haak, J., Molecular dynamics with coupling to an external bath. *J. Chem. Phys.* **1984,** *81*

(8), 3684-3690.

9. Essmann, U.; Perera, L.; Berkowitz, M. L.; Darden, T.; Lee, H.; Pedersen, L. G., A smooth particle mesh ewald method. *J. Chem. Phys.* **1995,** *103* (19), 8577-8593.

10. Kabsch, W.; Sander, C., Dictionary of protein secondary structure: pattern recognition of hydrogen-bonded and geometrical features. *Biopolymers* **1983,** *22* (12), 2577-2637.